Integrated Model of Transmission Tower Surge Impedance and Multilayer Grounding System Based on Full-wave Approach

M. Ghomi, H. Zhang, C. Leth Bak, F. Faria da Silva, K. Yin

***Abstract*—In this paper, a full-wave approach based on the method of moment (MoM) is proposed to investigate the harmonic impedance of a tower and its connected ground electrode in the frequency domain. The accuracy of the results is validated in comparison with NEC-4. The proposed numerical method is also employed for the evaluation of a full-sized HVDC tower harmonic impedance. The main contribution is the assessment of the harmonic impedance of a real tower with detailed geometrical information connected to the multi-layer grounding system. The validity of the transmission line method is evaluated through comparison with the results computed using the developed full-wave approach at the high frequency. In addition, the simulation results assure that a real tower's harmonic impedance could be smaller than the value estimated for very simplified models at the high frequencies. When the full-wave method is applied and the precise model of the ground electrode is considered, the harmonic impedance of the tower in the frequency domain and consequently, the transient impedance in the time domain are different, while the grounding system is assumed to be a perfectly conducting plane. These differences can become very significant, especially close to the resonant frequencies. The harmonic impedance of power transmission towers is strongly influenced by the connected grounding system.**

***Keywords*—Harmonic impedance, method of moment, multilayer grounding system, tower surge impedance.**

I. Introduction

ONE of the leading causes of a power transmission line (PTL) unscheduled outages are a lightning surges. Seven out of twelve significant blackouts that occurred in 2019 were reported to be due to a lightning strike to the PTLs [1]. The transient behavior of the transmission tower, which is struck by lightning, is vital in determining the basic impulse level (BIL). Accordingly, the detailed tower and grounding system modeling (GSM) are indispensable in the transient analysis. The lightning impulse is often specified by its wide-band frequency contents from dc to several MHz. The transient overvoltage quantities depend on some different parameters like lightning current waveform, GSM, mechanical specifications, construction, shield wire, and surge impedance characteristics of a tower or its transient impedance [2]. Significantly, the grounding system (GS) and the tower surge impedance (TSI) have considerable effects on the lightning performance of the PTLs. The available models of the tower in the Electromagnetic Transient Programs, such as ATP-EMTP [3] PSCAD/EMTDC [4], indicate some of the assumptions that limit its applicability at the high frequencies. Additionally, for the GSM, the resistive model has been utilized, which is not perfect for lightning studies. The tower impedance changes from the tower top to the tower bottom as the wave travels. A proper GS can provide a low-impedance path for the lightning currents into the soil to dampen the occurred transient overvoltages. However, the modeling of GSs is exceedingly difficult, because of its dynamic behaviors such as a multilayer structure [5], [6], and the frequency dependency of soil resistivity and permittivity [7]. The theoretical methods of the harmonic impedance calculation are based on quasi-static or full-wave approaches. The quasi-static techniques, such as circuit theory or transmission-line model (TLM) [8] fail to provide precise results when used for the estimation of the harmonic impedance. Also, the main limiting factor of the quasi-static approaches is low computational efficiency, which makes them prohibitively slow, in particular for the harmonic impedance calculations. The electrical dimensions of the problem should be much smaller than the smallest wavelength of the flowing current in the TLM. The full-wave methods can be presented as the most accurate results over a wide frequency range [9]. The numerical solution of Maxwell's equations can be performed using the finite element method (FEM) [10], the method of moments (MoM) [11], the finite-difference time-domain (FDTD) method [12]. The practical method is defined as a direct method in which an excitation current is injected at the top of the tower.

To estimate the surge impedance, several approaches have been using based on analytical and practical methods. It is worth noting that diverse expressions have been employed to determine the surge impedance, which was entirely dependent on the waveform of excitation current, the magnitude of the excitation current, and induced voltages. Hence, there is no agreement on the determination of surge impedance in the time domain [13].

In the time domain, tower transient behavior and the measured value of surge impedance are related to the angle and direction of excitation waveform [13], [16], and [18]. In the frequency domain, the harmonic impedance of the tower is a function of electromagnetic specifications and geometry of the system [13]. Therefore, using procedures based on the frequency domain is well suited to illustrate TSI [17]. The same approach for the tower surge impedance

M. Ghomi, H. Zhang, C. Leth Bak, and F. Faria da Silva, and K. Yin are with the Department of Energy technology, Aalborg University, Aalborg, Denmark (mhg@et.aau.dk; hazh@et.aau.dk clb@et.aau.dk; ffs@et.aau.dk; kyi@et.aau.dk).

Paper submitted to the International Conference on Power Systems Transients (IPST2021) in Belo Horizonte, Brazil June 6-10, 2021.

calculation has been used to appraise GS modeling. Therefore, among these techniques, MoM can be considered as an efficient approach in the frequency-domain because 1) it uses the thin-wire approximation with deducting two-dimensional surface integration to the one-dimensional line, 2) the harmonic impedance is not excitation waveform-dependent [18], [13]. To carry on with the attempts performed in [19], a numerical simulation is presented for harmonic impedance calculation of the integrated model. This model consists of detailed modeling of the tower and a GS in the frequency-domain unitedly.

This paper is organized as follows. In Section II, the developed full-wave approach is demonstrated concisely. The proposed method validation is investigated in Section III. The used delta-gap excitation model and the harmonic impedance analysis of the simple tower considering different GS configurations are shown in Section IV. Finally, the simulation results of the tower geometry impact on harmonic impedance considering multi-layer GS are analyzed as a proposed integrated model in Section V. Conclusion notes are described in Section VI.

II. Approach Description

This section is a general description of the theory of dielectric layers modeling and the procedure of MoM implementation [20]. The problem is defined by representing each layer with a thickness d, resistivity ρ_0, permittivity ε, and permeability μ. This procedure is based on the developed concept for appraisal of arbitrary microstrip structures in a multilayer medium [21].

Fig. 1 shows a three-layered medium which is separated by two planar interfaces. A vertical wire of length h along the z-axis of the multi-layer medium is considered [22]. The source and observation point could be assumed in any layer of interest. For mathematical modeling, the mixed-potential integral equation (MPIE) is utilized [23]. These potentials consist of vector and scalar. J_s is the current density on the surface S of the perfect electric conductors (PECs) placed in a layered media is obtained by applying boundary conditions on the surface of the elements of the model given in (1)

$$-\hat{a} \times E_s(r) = \hat{a} \times E_i(r) \tag{1}$$

where $E_i(r)$, $E_s(r)$, and r are the incident electric field, scattered field, and the position vector defined according to the rectangular coordinate system, respectively. The expression of electric current density $J_s(r)$ and surface charge density $\rho_s(r)$ are related to in (2)

$$\nabla . J_s(r) + j\omega\rho_s(r) = 0 \tag{2}$$

where ω and ρ_s are the angular frequency and density of electric charge, respectively. The MPIE formulation is obtained by fulfilling the boundary condition at the surface of elements and are given in (3)

$$E_s(r) = [-j\omega A(r) - \nabla V(r)] \tag{3}$$

where $A(r)$ and $V(r)$ being potential of magnetic vector and electric scalar potential, respectively. The gradient operator is ∇. By substituting (3) into (1) gives (4)

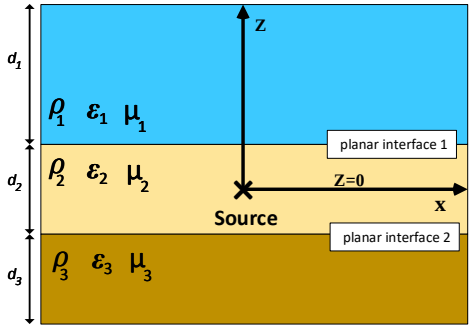

Fig. 1. Illustration of multi-layer medium.

$$\hat{a} \times [j\omega A(r) + \nabla V(r)] = \hat{a} \times E_i(r), \ r \text{ on } S \tag{4}$$

In this paper, the presented formula in (5) is selected as a Green's functions form for the magnetic vector potential [24]. The potentials could be explained in terms of Green's functions, which are obtained on the base of spectral-domain Green's functions for microstrip structures given in (6) and (7)

$$\overline{\boldsymbol{G}}_A = \begin{pmatrix} G_{xx} & G_{xy} & G_{xz} \\ G_{yx} & G_{yy} & 0 \\ G_{zx} & 0 & G_{zz} \end{pmatrix} \tag{5}$$

$$V(r) = \int_S \boldsymbol{G}_v(r \mid r')\, \rho_s(r')\, dS' \tag{6}$$

$$A(r) = \int_S \boldsymbol{G}_A(r \mid r') \cdot J_s(r')\, dS' \tag{7}$$

where $\boldsymbol{G}_A$ and $\boldsymbol{G}_v$ are magnetic vector and electric scalar potential Green's function, respectively. The spatial domain Green's functions are determined easily using inverse Fourier transform of its spectral pairs [24].

$$G_{A,v} = \frac{1}{2\pi} \int_0^{\infty} \tilde{G}_{A,v}(k_\lambda)\, J_0(k_\lambda \lambda)\, k_\lambda \mathrm{d}k_\lambda \tag{8}$$

where $k_\lambda = (k_x^2 + k_y^2)^{0.5}$, and k_x, k_y are wave vector components in the each layer on xy plane. ρ is J_0 is first kind Bessel's function, and $\tilde{G}_{A,v}$ is the Green's function for spectral domain [23]. The radial distance between the source segment and the point for calculating the electric field is λ. It should be pointed out that Sommerfeld integrals presented in (8) is solved numerically.

III. Model Verification

The validation of the models against experimental results is the most crucial part of the modeling. However, there has not been a comprehensive comparison between modeling and experimenting with the input impedance of towers connected to a ground electrode buried in multi-layer soil. The fundamental reasons for the lack of comparison are: 1) the measured voltage is path-dependent at the high frequencies between any two points, 2) there are complexities of measuring each layer's electrical parameters in a multi-layer soil structure. Due to the noted practical limitations for validation, NEC-4, as a widely accepted numerical electromagnetic code, is applied to investigating the presented method [25].

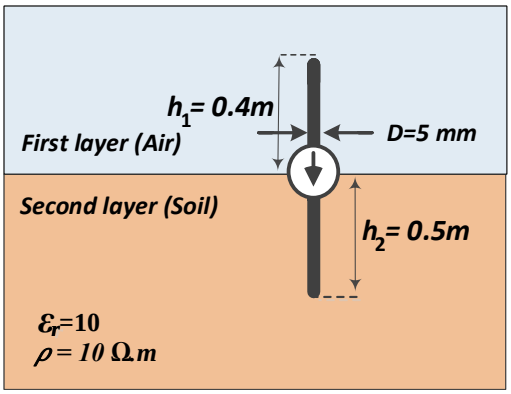

Fig. 2. Vertical electrode buried in soil which is connected to very simple tower.

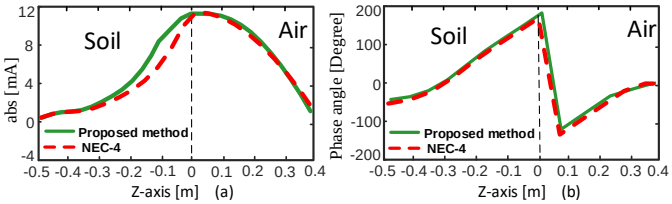

Fig. 3. Current distribution along the ground electrode and tower at 10 MHz. (a) absolute value (b) phase angle.

In this section, to verify the proposed method, a very simple case, consisting of a tower and vertical ground electrode (VGE), is applied. An antenna theory approach [13] is well suited to the frequency domain analysis of layered microstrip structures to calculate the Green's functions for multi-layer media, which are basically shown by Sommerfeld's integrals and formulas in the spatial and spectral domain, respectively.

Fig. 2 shows the tower geometrical configuration, and the junction point between the tower and ground electrode is used to excite the ground surface by a 1-V voltage source. A 0.4-m cylindrical tower with a 5-mm diameter is considered. The soil is characterized by a resistivity of 10 Ω.m and a relative permittivity of 10. This integrated model, tower, and GS are simulated numerically using a full-wave method.

Figs. 3(a) and (b) present the absolute value and phase angle of the current distribution vector along with the integrated model at higher frequencies, namely 10 MHz. The obtained results through NEC-4 are also illustrated in Fig. 3 along the z-axis. It can be seen that two methods predict similar behavior in the estimation of current distribution. This approach's usefulness is validated from the excellent consensus between the proposed method's results and computed results by NEC-4. It is seen that the proposed method can compute the distribution of current along with the integrated model precisely. The differences between absolute values in Fig. 3(a) refers to the selected basis function for the excitation source at the excitation terminal. The terminal is excited by an ideal voltage source of magnitude V_s in the integrated model. The triangular basis functions are employed. If $\delta \longrightarrow 0$, the induced terminal current passes into the ideal voltage source, and subsequently, it will expand to the half-subsectional basis function. An incident field is provided by the delta-gap voltage source at the excitation terminal.

IV. Analysis of Harmonic Impedance of the Integrated Model in the Frequency Domain

The most relevant contribution of lightning impulse for the outage rate of PTLs comes out from the tower surge impedance and the tower-footing GSs. The typical tower surge impedance characteristic and dynamic behavior of GSs are analyzed in detail elsewhere (e.g., [7]). According to the measurement expenses, complications of working on high-frequency phenomena, and the towers' diversity, few measurement results are presented. Also, the detailed information about the tested towers and their GS condition is not accessible. Numerical solvers are widely used to analyze the harmonic impedance of towers and GSs.

A. Harmonic Impedance Calculation Based on MoM

The harmonic impedance is extremely helpful in the transient analysis. It is given by (9)

$$Z_{input}(f) = \frac{V(f)}{I(f)} \tag{9}$$

where $I(f)$ and $V(f)$ are phasors of the injected current and the steady-state harmonic electric potential at the injection point in reference to the remote terminal, respectively(see [29], [31]). It depends on the electromagnetic characteristics and the geometry of the medium, and not on excitation. The input harmonic impedance of the integrated model can be calculated from the MoM matrix directly. Based on MoM, a full-wave frequency-domain approach, the integrated model is divided into N small segments. Accordingly, a lower number of segments needs to be taken into account (see [24]).

1) Excitation Model: Two theoretical models can be applied to an excitation source modeling, namely, delta-gap and impressed current models [26]. In this part, the modeling of the delta-gap excitation approach is reviewed concisely. According to the presented model in [26], the tower is excited by the voltage source V_s, applied within a tiny gap region of length $\delta \longrightarrow 0$ and across the reference plate (perfect electric conductor (PEC)) and the excitation terminal (see Fig. 4(a)). To obtain finite input impedance, a nontrivial voltage must always be induced across the gap, which has a width of almost zero. Thin wire approximation is employed to compute the distributed currents along all conductors in the mentioned case. To avoid the first segment current discontinuity, the first segment is utilized to create the induced terminal current at each frequency. Within the MoM methodology, Fig. 4(b) shows the expanded finite series of current distribution on the surface of conductors, which is located on the multi-layer medium. To solve (4), the electric current density on the conductors surface (tower and vertical ground electrode) can be defined as follow:

$$J_s(r') = I^t f_t(r') + \sum_{n=1}^{N} I^c f_n(r') \tag{10}$$

where the half-subsectional basis function, $f_t(r')$, generates terminal current and $f_n(r')$ represents full-subsection basis functions. I^t and I^c denote the induced current coefficient that is associated with half-subsectional basis function and the unknown coefficients that are associated with the triangular

basis functions, respectively [27]. The voltage source of the delta gap at the tower top creates the incident excitation field given by (11)

$$E_i = V_s \delta (r - r') \hat{a} \tag{11}$$

where r' is the terminal and r is the distance along with the integrated model. As presented in Fig. 4(b), the induced terminal current, I^t, goes along the voltage source, which expands into a half-subsectional basis function, also located at r_n. The identical MPIE governing the surface current, J_s, on the surfaces of the integrated model conductors is given by (12)

$$\int G_A (r \mid r') \cdot J_S (r') \, dS' + V_s \delta (r - r') \hat{a} = 0 \tag{12}$$

2) Integration Path Influence on the harmonic Impedance: It is well known that the voltage between two points along a determined path in the general case is given by (13)

$$V_s = \int_s \overrightarrow{E}_{total} \cdot \overrightarrow{dl} = \Delta V(r) - \frac{\partial}{\partial t} \int \vec{A} \cdot \overrightarrow{dl} \tag{13}$$

$$\overrightarrow{E}_{total} = \overrightarrow{E}_i + \overrightarrow{E_s} \tag{14}$$

where S shows the integration path on the excitation terminal. In the case of an electrostatic field, the voltage value is not dependent on the integration path and it is unique. Once the current distribution has been computed along with the components, the electric field can be computed at any point by summing the contributions due to the currents in each segment. In this situation, the last term of (13) is zero and the voltage is exactly different from electric scalar potentials.

Generally speaking, for a dynamic electromagnetic field, the electric field is not conservative and the integral of the electric field between any two points is path-dependent. Due to this issue and to determine a unique voltage, the gradient of the scalar potential calculated along a unique straight path extends to the remote ground reference point. The path-dependent voltage is estimated by (15) expression based on Faraday's law.

$$V^{'}(r) - V(r) = \frac{\partial}{\partial t} \int \vec{B} \cdot \overrightarrow{dS} \tag{15}$$

where $V^{'}(r)$, $V(r)$, and B are voltages obtained along a path on S and magnetic flux density, respectively. The input impedance at the excitation terminal is calculated as follows:

$$Z_{input}(f) = \frac{V_s}{I^t} = -\frac{\int_S \overrightarrow{E}_{total} \cdot \overrightarrow{dl}}{I^t} \tag{16}$$

One way to circumvent the problem of path dependence is to use the scalar potential instead of the voltage as the integral of the electric field over a given path. Such an approach has the benefit that the scalar potential is uniquely derived. Hence, with this assumption, the voltage or the integrated value is independent of the integration path [13]. Adaptive Simpson's integration is employed to evaluate the integrals over the finite interval, while Mosig's method of averages is applied to assess the integrals over the infinite interval, which features a very fast convergence [32].

3) Terminal Length Effect on the Harmonic Impedance: The presence of the excitation terminal can create a parasitic inductance [30]. It can be estimated by (17)

TABLE I
EXCITATION TERMINAL IMPEDANCE MAGNITUDE

Terminal Length (mm)	Impedance (Ω)
10	0.10484
50	1.25520
100	3.31200
1000	61.4200

$$L = 0.2 \times h \times \left(\ln \frac{2h}{b} + \frac{0.223b}{h} + 0.5 \right) [nH] \tag{17}$$

where h and b are the length and width of the excitation terminal in mm, respectively. For instance, for a conductor radius of 12.5 mm, the port width is set to 25 mm. The terminal's impedance magnitude (ωL) for several port lengths in the maximum frequency of 10 MHz is given in Table I. This table shows that to achieve a negligible impedance, the excitation terminal length must be no longer than 100 mm. This length is considered for the excitation segment.

4) Moment Impedance Matrix: In this part, the impedance matrix of the system is obtained by making use of the MoM solution to Maxwell's equations. Maxwell's equations are reduced to a matrix form by applying to (12). The electric field at the observation point will be computed once finding the current of each segment. The moment impedance matrix is defined by (18). Also, the impedance matrix can be expressed by (19). Eventually, by formulating the problem as a close form matrix, given by (20), unknown coefficients vector is computed [27].

$$\begin{pmatrix} Z_{1,1} & \cdots & Z_{1,N+1} \\ \vdots & \ddots & \vdots \\ Z_{1+N,1} & \cdots & Z_{1+N,N+1} \end{pmatrix} \begin{pmatrix} I^t \\ \vdots \\ 0 \end{pmatrix} = \begin{pmatrix} V_s \\ \vdots \\ 0 \end{pmatrix} \tag{18}$$

$$\begin{pmatrix} Z^{tt} & Z^{tc} \\ Z^{ct} & Z^{cc} \end{pmatrix} \begin{pmatrix} I^t \\ I^c \end{pmatrix} = \begin{pmatrix} V_s \\ 0 \end{pmatrix} \tag{19}$$

where $Z^{ii}(f)$ and $Z^{ij}(f)$ represent self and mutual impedance, respectively which $i, j \in \{t, c\}$. I^c can be obtained from the following resultant matrix equations:

$$[z][I] = [V_s] \tag{20}$$

where $[z]$,$[I]$, and $[V_s]$ are the moment impedance matrix, the unknown coefficients vector, and the excitation vector, respectively. Finally, for the wide frequency range, the relation between the terminal voltage and induced current in an impedance matrix form is obtained from the moment impedance matrix by manipulation of (19). Z_{input} is given as follow:

$$Z_{\text{input}}(f) = Z^{tt}(f) - Z^{tc}(f) \left(Z^{cc}(f) \right)^{-1} Z^{ct}(f) \tag{21}$$

where $Z_{\text{input}}(f)$ is the calculated harmonic impedance. From Fig. 6, the proposed method for calculating long integration path harmonic impedance converges to the impedance estimated by the conventional method for long integration path.

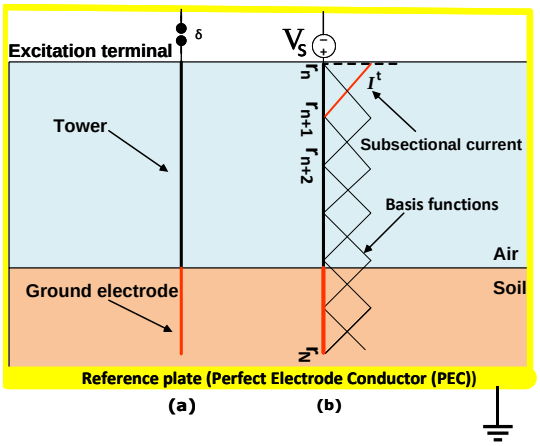

Fig. 4. Setup for the calculation of harmonic impedance of the integrated model. (a) delta-gap excitation generator, (b) triangular basis functions, and the segmented integrated model.

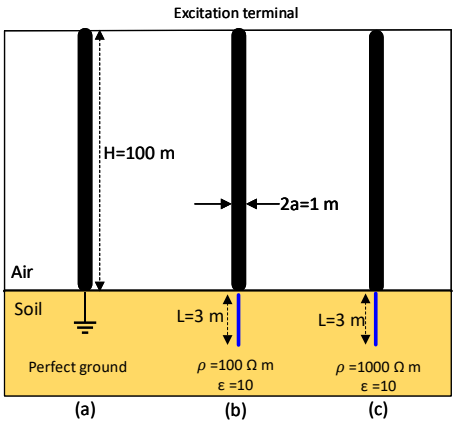

Fig. 5. Geometry of the two-layer medium. (a) tower end is connected to PEC adapted from [13], (b) integrated model which tower end is connected to vertical electrode buried in soil resistivity of 100 Ωm, and (c) resistivity of 1000 Ωm.

B. Grounding System Effect on Integrated Model Harmonic Impedance

To assess the GS effect on the harmonic impedance of a tower, a cylindrical tower is considered. The specification of this case is adapted from [13]. The configurations are shown in Fig. 5. The tower is placed in the upper layer, and the depth of the first layer is equal to the tower length. The upper layer medium is an air, which is supposed to be lossless and characterized by magnetic permeability μ_0 and permittivity ε_0. The input impedance of the problem is calculated with and without a real model of the GS. The end of the tower is connected to the zero-potential ground, PEC (see Fig. 5(a)), and in the Figs. 5(b) and (c), the tower is connected to the VGE length of 3-m buried in soil with a resistivity of 100 and 1000 Ωm, respectively. The related permittivity of soil is set to 10.

To further appraise the impact of the integration path on the harmonic impedance, various lengths (0.5, 2, 50, 100-m) of the integration path are taken into account. The harmonic impedance of the integrated model is illustrated in Fig. 6. It is clear from the figure that the harmonic impedance strongly depends on the length of the integration path (Paths in Fig. 6). In this paper, the concept of remote terminal voltage which is presented by $Grcev$ as a scalar potential [13] is used for validating the calculated harmonic impedance of the integrated model, which was presented as a direct characterization in Section IV-A-4. The corresponding voltage for the $infinity$ case is almost equivalent to the scalar potential. The path-dependence effect on harmonic impedance is visible at frequencies under 700 kHz. It is clear that the applied method must be rigorously checked for the impact of path dependency on the harmonic impedance.

Fig. 7 shows the obtained harmonic impedance using TLM and MoM, which have the same results up to the first frequency (FRF) of 0.75 MHz when assuming a PEC. The full-wave approach can calculate the minimum and maximum values of input harmonic impedance at the higher frequencies more accurately than the TLM method, which does not calculate zero or infinite accurately. The high deviations at the specific frequencies may be attributed to radiation loss, which the full-wave model considers. The TLM method does not consider the mutual coupling between the adjacent segments, so it is expected that they might lead to differences in the high-frequency response. In the TLM, the VGE is supposed to have zero resistivity and the tower is simulated by a surge impedance whose value is calculated by (22)

$$Z_c = 60 \ln \frac{H_{tower}}{a_{tower}} \tag{22}$$

where H_{tower} and a_{tower} are the height and radius of the tower in meters, respectively. Z_c has a value of 317.9 Ω for the tower radius of 0.5 m and the tower height of 100 m [13], [15]. The detailed formulation of the grounding system modeling using the TLM can be found in [14]. It is assumed that the 3-m vertical electrode is buried in the soil with two different resistivities of [ρ= 100 Ω.m, Fig. 5(b)] and [ρ= 1000 Ω.m, Fig. 5(c)]. The influence of an accurate model of the GS on the input impedance is illustrated. It may be noted in Figs. 7 and 8 that the TLM model greatly overestimates the values of harmonic impedance at high frequencies. Also, the harmonic impedance of the integrated model has a different behavior from the estimated harmonic impedance of the tower, which is connected to the perfect GS. This dissimilarity at the frequency of resonance and different behavior at high frequency may be ascribed to change system transfer function in the frequency domain and radiation losses. The subsequent stroke impulse with a larger front rise rate has higher frequency contents in comparison with the first stroke impulse [29]. It is worth noting that the use of the TLM could be revised principally at the lightning studies [13].

V. Impact of Tower Geometry on Harmonic Impedance Considering Multilayer Soil

In this section, to further assess the applicability of the proposed integrated model, the input impedance of the typical full-sized HVDC tower is investigated compared to an approximated model of the towers in the frequency domain [17]. The tower is simulated with three levels of detail. Firstly, in a very simplified model, only the main cylinder with a height of 89.5 m and simple cross arm is

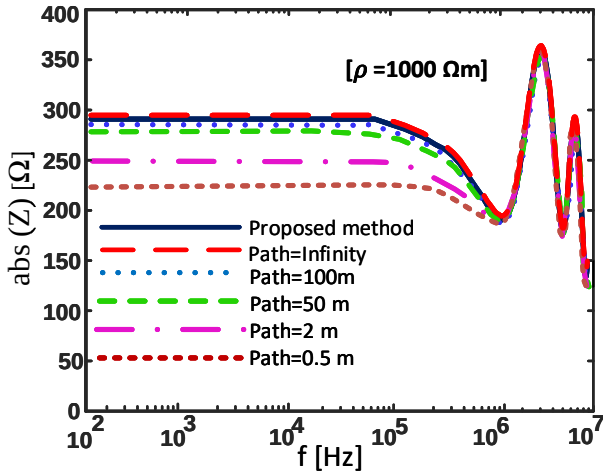

Fig. 6. Integration path effect on the harmonic impedance absolute value of integrated model shown in Fig. 5(c) [ρ= 1000 Ωm].

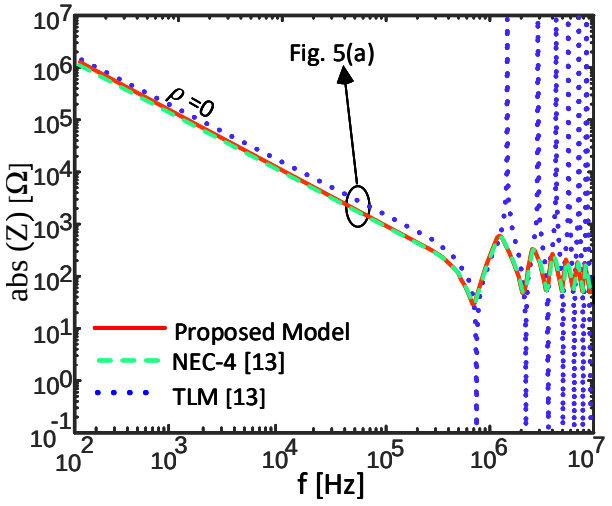

Fig. 7. Geometry of the two-layer medium. (a) tower end is connected to PEC adapted from [13], (b) integrated model which tower end is connected to vertical electrode buried in soil resistivity of 100 Ωm, and (c) resistivity of 1000 Ωm.

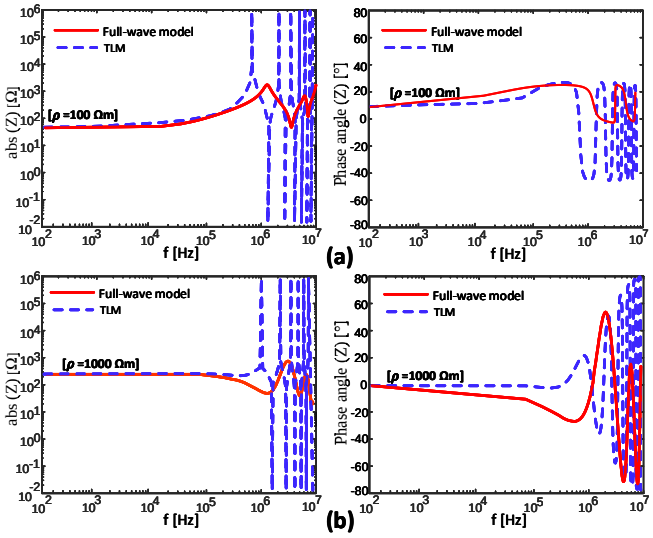

Fig. 8. Harmonic impedance of tower and its connected VGE [absolute value (left column) and phase angel (right column)] shown in Fig. 5(b) [ρ= 100 Ωm] and Fig. 5(c) [ρ= 1000 Ωm]. Full-wave model: red line, TLM model: blue dashed line.

considered [$tower(a)$, Fig. 9(a)]. Next, the simplified model, four legs and cross arm with the width of 20 m are added to the geometry [$tower(b)$, Fig. 9(b)]. Finally, all members and components of the steel lattices tower are taken into account in [($tower(c)$, Fig. 9(c)] as a complex model. The equivalent model of the presented integrated model in the frequency domain, the medium of the integrated model, and the top view of the real tower are shown, respectively in Figs. 9(d), (e), and (f). For each case, the harmonic impedance is calculated up to 10 MHz. The full-wave method based on MoM solutions to Maxwell's equations is used for evaluating the harmonic impedance observed from the tower top. This model has been extensively used to determine the transient surge impedance in lightning studies. It is worth noting that the real tower structure is much more complicated compared with the very simple equivalents (see Fig. 9) [28]. The influence of the tower elements on the harmonic impedance with an accurate model of GS is analyzed unitedly in this study.

All towers are connected to the VGE buried in uniform and multilayer soil structures. To this aim, two configurations of the soil layers are defined in Table II with resistance values of 100 and 1000 Ωm. A soil permittivity is set to 10 for all cases. The electrode is 3-m long and has a diameter of 30 mm. The input impedance seen from the tower top is determined as the harmonic impedance in the frequency domain, as explained in section IV-B.

Fig. 10 shows simulation results of the computed harmonic impedance of the tower, which is connected to the VGE with the adopted parameters in Table II for case 1. In this case, the maximum value of harmonic impedance magnitude for the presented tower has a noticeable difference between the simplified towers (tower (a) and (b)) and the complex model of the tower.

For case 2, the soil is characterized by the resistivity of 1000 Ωm. Towers are connected to this GS. According to Fig. 10, the obtained harmonic impedance of a very simplified tower is markedly higher than the obtained results for Figs. 9(b) and (c). The peak values of the harmonic impedance magnitude are 23 and 140 for cases 1 and 2, respectively. The LF harmonic impedance is the same for all towers in each case. The values of R_{LF} are 33.9 and 313 Ω for the case of 1 and 2, respectively. It can be seen that all towers have the same response at low frequencies up to FRF. For instance, in case 1, the FRF value is different and changes from 1.4 MHz for the tower (a) to 0.92 MHz for the tower (c). It varies from 1.2 MHz for the tower (a) to 1 MHz for the tower (c) in case 2.

To further analyze the influence of the tower-footing GS on the harmonic impedance of the integrated model, the same VGE with a length of 3-m buried in a multi-layer soil is taken into account in cases of 3 and 4. The upper soil layer depth is set to d_2 =1m. The electrical parameters of soil are given in Table II. The obtained results associated with the harmonic impedance (amplitude and phase angle) observed from the tower top are shown in Fig. V.

For case 3, the maximum value of harmonic impedance magnitude is significantly distinct between the illustrated towers in Fig. 9. The maximum value of input impedance for the tower in Fig. 9(a) has appeared in the second resonant

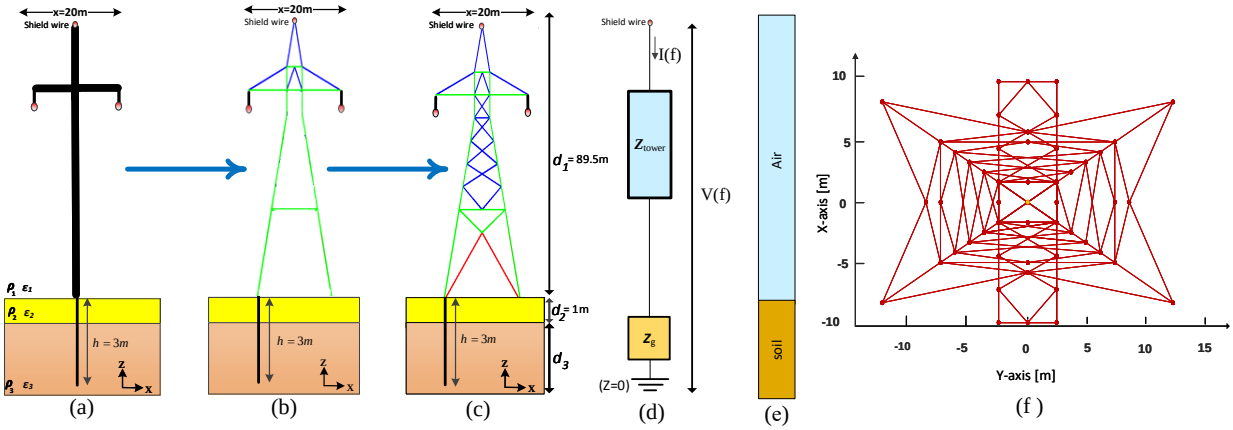

Fig. 9. HVDC tower side view. (a) very simplified structure, (b) simplified structure, (c) real tower, (d) frequency-dependent representation of tower which is connected to the ground electrode, (e) medium of integrated model, (f) 2-D top view of the simulated real tower in the X-Y plane.

TABLE II
ADOPTED VALUES OF THE SOIL RESISTIVITY

Ground structures	$\rho_1(\Omega.m)$	$\rho_2(\Omega.m)$
Case 1 (uniform soil)	100	100
Case 2 (uniform soil)	1000	1000
Case 3 (multilayer soil)	100	1000
Case 4 (multilayer soil)	1000	100

frequency at 4MHz, but the peak value of the harmonic impedance of the complex tower model occurs at 6 MHz. The results show different behavior for the simplified and complex models depending on the differences related to the maximum values of harmonic impedance at resonance frequencies [see Fig. V(a)]. A predicted impedance using a full-wave approach might be smaller than the predicted values for a very simplified tower. Differences could become very significant, especially close resonant frequencies.

To supplementary evaluate the effect of the buried VGE in multi-layer soil on the integrated model harmonic impedance, the upper and lower soil layers are, respectively, characterized by resistivity of ρ_1=1000Ωm and ρ_2=100Ωm, both having the same relative electric permittivity of 10. (see case 4 in Table II). The magnitude and phase angle of the harmonic impedance of this case is demonstrated in Fig. V(b). From the results shown here, it is observed that the harmonic impedance is a function of different parameters such as the tower's geometry and electromagnetic characteristics of medium and tower footing GS specifications. The influence of the tower elements and the exact model of the GS on the peak value of harmonic impedance magnitude is briefly presented in Table III.

VI. CONCLUSIONS

This paper can be regarded as a continuation of the work developed by *Grcev* and *Ametani* in [13] and [17]. A precise full-wave MoM-based solution of Maxwell's equations for calculating the harmonic impedance's integrated model was proposed. The contributions of this paper are listed as follows:

a) A comprehensive methodology based on the full-wave approach was introduced, which can directly provide the integrated model's harmonic impedance consisting of a tower and grounding system.

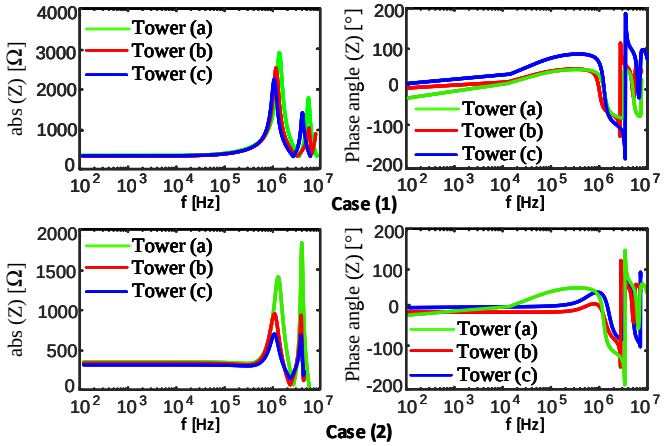

Fig. 10. Influence of tower model on the harmonic impedance [absolute value and phase angle] of the integrated model. The ground electrode of towers is buried in the uniform soil (see cases 1 and 2 in Table II).

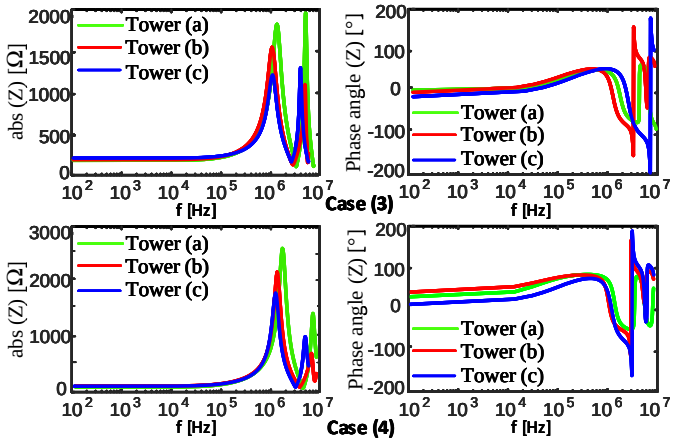

Fig. 11. Influence of a tower model on harmonic impedance [absolute value and phase angle] of the integrated model. The ground electrode of towers is buried in the multilayer soil (see cases 3 and 4 in Table II)

b) The impedance vectors, including the self and mutual impedances, are calculated in the multi-layer medium using MoM matrix directly, which differs from the approach adopted in [13] and [17].

c) Simulations are implemented to solve the full-wave Maxwell's equations regarding the tower's detailed model and

TABLE III
COMPARISON OF MAX. VALUES OF THE INTEGRATED MODEL INPUT IMPEDANCE

Cases	$R_{LF}[\Omega]$	$\lvert Z\rvert_m[\Omega]$ (a)	(b)	(c)	%diff($\lvert Z\rvert_m$)	FRF(MHz) (a)	(b)	(c)
1	33.9	2924	2650	2371	23	1.4	1.13	0.92
2	313	1828	963	759	140	1.2	0.95	1
3	93.5	2070	1530	1315	57	1.7	0.91	1.02
4	42.6	2576	2275	1751	47	1.8	1	1.1

the grounding system's real geometry.

d) The correctness of the theoretical procedure, TLM, is examined through comparison with the obtained results of the integrated model based on the developed full-wave approach.

e) In all cases, (tower (a) and (b)), overestimate the peak value of the harmonic impedance in comparison to the detailed model at the specific frequencies. However, the input harmonic impedance of the tower in the frequency domain, and consequently, the transient impedance in the time domain, was different as long as the GS is assumed a perfectly conducting plane. The related differences for cases 1, 2, 3, and 4 are 23, 140, 57, and 47% in the frequency domain. It can bring about notable errors in transient impedance values in the time domain.

f) The frequencies of resonance, the minimum and maximum values of the harmonic impedance, varied when the system transfer function is changed based on the GS model.

g) The exact model of the tower and grounding system could be necessary for the back-flashover rate approximation and other surge performances associated with the PTLs. These are significant factors in optimizing the cost of insulation coordination and the protection systems.

VII. REFERENCES

[1] List of major power outages," https://en.wikipedia.org/wiki/List of major power outages.

[2] L. Grcev and M. Popov, "On high-frequency circuit equivalents of a vertical ground rod," IEEE Trans. Power Del., vol. 20, no. 2, pp. 1598–1603, Apr. 2005.

[3] J. Mahseredjian, S. Dennetiere, L. Dube, B. Khodabakhchian, and L. Gerin-Lajoie, "On a new approach for the simulation of transients in power systems," Elect. Power Syst. Res., vol. 77, no. 11, pp. 1514–1514, Sep. 2007.

[4] "PSCAD/EMTDC User's Manual: Ver.4.2," Manitoba HVDC Research Centre, 2005.

[5] M. Ghomi, H. Mohammadi, and H. Karami, "Full-wave modeling of grounding system:Evaluation the effects of multi-layer soil and length of electrode on ground potential rise," International Conference on Power Systems Transients, IPST, pp. 1–6, 2019.

[6] M Ghomi, C Leth Bak, F Faria da Silva," Frequency Dependence of Multilayer Soil Electrical Parameters: Effects on the Input Impedance of Grounding Systems," 16th International conference on AC and DC power transmission.ACDC 2020.

[7] A. Ametani, Y. Kasai, J. Sawada, A. Mochizuki, and T. Yamada, "Frequency-dependent impedance of vertical conductors and a multiconductor tower model," Proc. Inst. Elect. Eng., Gen., Transm. Dist., vol.141, pp. 339–345, July 1994.

[8] Z. Feng, X. Wen, and X. Tong, "Impulse characteristics of tower grounding devices considering soil ionization by the time-domain difference method," IEEE Transactions on Power Delivery, vol. 30, no. 4, pp. 1906-1913, 2015.

[9] M. A. Sargent and M. Darveniza, "Tower surge impedance," IEEE Trans. Power App. Syst., vol. PAS-88, pp. 680–687, May 1969.

[10] A. Sunjerga, F. Rachidi, and M. Rubinstein, "Calculation of the grounding resistance of structures located on elevated terrain," IEEE Transactions on Electromagnetic Compatibility, pp. 1-5, 2018.

[11] L. Grcev, A. Kuhar, and V. Arnautovski-Tasova, "Evaluation of high-frequency circuit models for horizontal and vertical grounding electrodes," IEEE Transactions on Power Delivery, vol. 33, no. 6, pp. 3065-3074, 2018.

[12] Y. Baba, N. Nagaoka, and A. Ametani, "Modeling of thin wires in a lossy medium for FDTD simulations," IEEE Transactions on Electromagnetic Compatibility, vol. 47, no. 1, pp. 54-60, 2005.

[13] L. Grcev and F. Rachidi, "On tower impedances for transient analysis," in IEEE Transactions on Power Delivery, vol. 19, no. 3, pp. 1238-1244, July 2004.

[14] C. R. Paul, Analysis of multiconductor transmission lines. IEEE Press, 2007.

[15] CIGRE WG01 SC33, to procedures for estimating the lightning performance of transmission lines, A. Eriksson (CH), L. Dellera (IT), G. Baldo (IT), C. H. Bouquegneau (BE), H. Darvenisa (AU), J. Elovaara (FI), E. Garbagnati (IT), C. Gary (FR)," Cigre Tb 63, vol. 01, no. October, p. 64, 1991.

[16] H. Motoyama, Y. Kinoshita, K. Nonaka and Y. Baba, "Experimental and Analytical Studies on Lightning Surge Response of 500-kV Transmission Tower," in IEEE Transactions on Power Delivery, vol. 24, no. 4, pp. 2232-2239, Oct. 2009.

[17] A. Ametani, N. Triruttanapiruk, K. Yamamoto, Y. Baba and F. Rachidi, "Impedance and Admittance Formulas for a Multistair Model of Transmission Towers," in IEEE Transactions on Electromagnetic Compatibility, doi: 10.1109/TEMC.2020.2976644.

[18] B. Salarieh, H. M. J. De Silva, A. M. Gole, A. Ametani and B. Kordi, "An Electromagnetic Model for the Calculation of Tower Surge Impedance Based on Thin Wire Approximation," in IEEE Transactions on Power Delivery, vol. 36, no. 2, pp. 1173-1182, April 2021.

[19] T. Noda and S. Yokoyama, "Thin wire representation in finite difference time domain surge simulation," IEEE Trans. Power Del., vol. 17, no. 3, pp. 840–847, Jul. 2002.

[20] K. A. Michalski and D. Zheng, "Electromagnetic scattering and radiation by surfaces of arbitrary shape in layered media. I. Theory," in IEEE Transactions on Antennas and Propagation, vol. 38, no. 3, pp. 335-344, March 1990.

[21] K. A. Michalski and D. Zheng, "Electromagnetic scattering and radiation by surfaces of arbitrary shape in layered media. II. Implementation and results for contiguous half-spaces," in IEEE Transactions on Antennas and Propagation, vol. 38, no. 3, pp. 345-352, March 1990.

[22] B. Markovski, L. Grcev and V. Arnautovski-Toseva, "Fast and Accurate Transient Analysis of Large Grounding Systems in Multilayer Soil," in IEEE Transactions on Power Delivery, doi: 10.1109/TPWRD.2020.2985926.

[23] J. R. Mosig and F. E. Gardiol, "Analytical and numerical techniques in the Green's function treatment of microstrip antennas and scatterers," IEE Proc. HMicrow., Opt. Antennas, vol. 130, no. 2, pp. 175–182, Mar. 1983.

[24] G. Dural and M. I. Aksun, "Closed-form green's functions for general sources and stratified media," IEEE Trans. Microw. Theory Tech., vol. 43, no. 7, pp. 1545–1552, Jul. 1995.

[25] G. J. Burke, "Numerical electromagnetic code (NEC-4), method of moments," Lawrence Livermore Nat. Lab., Livermore, CA, USA, UCRL-MA-109338, 1992.

[26] G. V. Eleftheriades and J. R. Mosig, "On the network characterization of planar passive circuits using the method of moments," IEEETrans. Microw. Theory Techn., vol. 44, no. 3, pp. 438–445, Mar. 1996.

[27] L. Grcev, "Modeling of grounding electrodes under lightning currents," IEEE Trans. Electromagn. Compat., vol. 51, no. 3, pp. 559–571, Aug. 2009.

[28] M. Ishii and Y. Baba, "Numerical electromagnetic field analysis of tower surge response," in IEEE Transactions on Power Delivery, vol. 12, no. 1, pp. 483-488, Jan. 1997, doi: 10.1109/61.568275.

[29] L. Grcev, "Impulse efficiency of ground electrodes," IEEE Trans. Power Del., vol. 42, no. 24, pp. 441–451, Jan. 2009.

[30] C. R. Paul, "Inductance: Loop and Partial," Wiley-IEEE Press, 2010.

[31] F. P. Dawalibi, W. Ruan, S. Fortin, J. Ma and W. K. Daily, "Computation of power line structure surge impedances using the electromagnetic field method," 2001 IEEE/PES Transmission and Distribution Conference and Exposition. Developing New Perspectives (Cat. No.01CH37294), Atlanta, GA, USA, 2001, pp. 663-668 vol.2.

[32] J. R. Mosig and T. K. Sarkar, "Comparison of quasi-static and exact electromagnetic fields from a horizontal electric dipole above a lossy dielectric backed by an imperfect ground plane," IEEE Trans. Microw. Theory Tech., vol. MTT-34, no. 4, pp. 379–387, Apr. 1986.